SN 2011A: A LOW-LUMINOSITY INTERACTING TRANSIENT WITH A DOUBLE PLATEAU AND STRONG SODIUM ABSORPTION*

T. de Jaeger[1,2], J. P. Anderson[3], G. Pignata[1,4], M. Hamuy[1,2], E. Kankare[5], M. D. Stritzinger[6], S. Benetti[7], F. Bufano[1,4], N. Elias-Rosa[7,8], G. Folatelli[9,10], F. Förster[1], S. González-Gaitán[1,3], C. P. Gutiérrez[1,2,3], C. Inserra[5], R. Kotak[5], P. Lira[2], N. Morrell[11], F. Taddia[12], and L. Tomasella[7]

[1] Millennium Institute of Astrophysics, Casilla 36-D, Santiago, Chile; dthomas@das.uchile.cl
[2] Departamento de Astronomía—Universidad de Chile, Camino el Observatorio 1515, Santiago, Chile
[3] European Southern Observatory, Alonso de Cordova 3107, Vitacura, Santiago, Chile
[4] Departamento de Ciencias Físicas—Universidad Andres Bello, Avda. República 252, Santiago, Chile
[5] Astrophysics Research Center, School of Mathematics and Physics, Queens University Belfast, Belfast, BT7 1NN, UK
[6] Department of Physics and Astronomy, Aarhus University, Ny Munkegade 120, DK-8000 Aarhus C, Denmark
[7] INAF–Osservatorio Astronomico di Padova, vicolo dell'Osservatorio 5, I-35122, Padova, Italia
[8] Institut de Ciències de l'Espai (IEEC-CSIC), Facultat de Ciències, Campus UAB, 08193 Bellaterra, Spain
[9] Instituto de Astrofsica de La Plata, CONICET, Paseo del Bosque S/N, B1900FWA, La Plata, Argentina
[10] Kavli Institute for the Physics and Mathematics of the Universe (WPI), Todai Institutes for Advanced Study,
the University of Tokyo, Kashiwa, 277-8583, Japan (Kavli IPMU, WPI)
[11] Las Campanas Observatory, Carnegie Observatories, Casilla 601, La Serena, Chile
[12] The Oskar Klein Centre, Department of Astronomy, Stockholm University, AlbaNova, SE-10691 Stockholm, Sweden

ABSTRACT

We present optical photometry and spectroscopy of the optical transient SN 2011A. Our data span 140 days after discovery including *BVRI u'g'r'i'z'* photometry and 11 epochs of optical spectroscopy. Originally classified as a type IIn supernova (SN IIn) due to the presence of narrow Hα emission, this object shows exceptional characteristics. First, the light curve shows a double plateau, a property only observed before in the impostor SN 1997bs. Second, SN 2011A has a very low luminosity ($M_V = -15.72$), placing it between normal luminous SNe IIn and SN impostors. Third, SN 2011A shows low velocity and high equivalent width absorption close to the sodium doublet, which increases with time and is most likely of circumstellar origin. This evolution is also accompanied by a change in line profile; when the absorption becomes stronger, a P Cygni profile appears. We discuss SN 2011A in the context of interacting SNe IIn and SN impostors, which appears to confirm the uniqueness of this transient. While we favor an impostor origin for SN 2011A, we highlight the difficulty in differentiating between terminal and non-terminal interacting transients.

Key words: circumstellar matter – stars: mass loss – supernovae: general – supernovae: individual (2011A)

1. INTRODUCTION

It is generally accepted that the majority of massive stars with zero-age main sequence masses $\geqslant 8\ M_\odot$ (Smartt 2009) end their lives as core-collapse supernovae (CC SNe), with the possibility that some directly form black holes with no visible supernovae (Smartt 2015). CC SNe are classified in two groups according to the absence (SNe Ib/c) or presence (SNe II) of H I lines (Filippenko 1997). The ejected material from an SN explosion is sometimes observed to interact with surrounding circumstellar material (CSM), related to progenitor mass-loss episodes prior to explosion (Chevalier 1981; Fransson 1982).

When the CSM is sufficiently dense, a strong CSM–ejecta interaction can begin shortly after explosion; this is often observed as a type IIn supernova (SN IIn henceforth; Schlegel 1990; Chugai & Danziger 1994). These objects are characterized by prevalent blue continua and narrow emission lines in their spectra superimposed on broader emission profiles. The Hα emission typically dominates the spectrum and often has multiple components consisting of the following (e.g., Salamanca et al. 1998).

1. Narrow emission ($v_{\mathrm{FWHM}} \sim$ few hundred km s^{-1}) formed by the photoionization of the high density pre-existing CSM from the prompt emission of the SN. The high density has furthermore been attributed to a high mass-loss rate (Chugai et al. 2004).
2. Intermediate emission ($v_{\mathrm{FWHM}} \sim$ few thousand km s^{-1}) possibly produced from the shock interaction of the SN blast within a dense shell of clumpy CSM or with a dense equatorial wind (Chugai & Danziger 1994).
3. Broad emission ($v_{\mathrm{FWHM}} \gtrsim 10^4$ km s^{-1}) most likely due to SN ejecta as a result of multiple scattering by thermal electrons in the opaque CS gas (Chugai 2001). The presence of this broad Hα emission without broad

P Cygni absorption is usually considered to be caused by a dense wind (Chugai 1990).

Measured parameters of these components can provide valuable information on progenitor properties and late time evolution (such as the mass-loss rate or wind velocity), through the observed properties of their CSM.

Observations of SNe IIn published to date (see, e.g., Kiewe et al. 2012; Zhang et al. 2012; Taddia et al. 2013) have allowed researchers to probe the immediate environment of these explosions and point toward significant diversity among various SNe IIn. The high mass-loss rates calculated from the observations of various SNe IIn (e.g., Kiewe et al. 2012; Taddia et al. 2013; Moriya et al. 2014) have prompted several authors to assign luminous blue variable stars (LBVs) in several cases as immediate progenitors of SNe IIn. LBVs, as defined by Humphreys & Davidson (1994), are some of the most luminous stars, with episodic and violent mass-loss events with mass-loss rates $\geqslant 10^{-3} M_\odot$ yr^{-1}. Classic examples of LBVs are Eta Carinae and P Cygni. Direct detection of the extremely luminous progenitor of SN 2005gl (Gal-Yam & Leonard 2009) also supports this possibility. However, in stellar evolutionary models, the LBV phase follows a blue giant star state (Crowther 2007; Gräfener & Hamann 2008), most likely with mass loss driven by the bi-stability jump (Vink 2011), and it is then followed by a H-poor WN star (nitrogen-rich Wolf–Rayet). In this scenario the LBV star loses its H envelope, becomes a Wolf–Rayet star, and then explodes as an SN. Thus, LBVs have been placed in the post-main sequence, but not the final pre-SN phase (Schaller et al. 1992; Langer 1993; Stothers & Chin 1996; Maeder et al. 2005; Maeder & Meynet 2008; Dwarkadas et al. 2010), but see Groh et al. (2013) for recent modeling suggesting that some stars could indeed end their lives during this phase.

There have been a number of cases where transients have originally been defined as SNe IIn, but the link to a definitive SN event (i.e., the terminal stage of a star's life) is questionable. Such events have been defined as SN "impostors" (Van Dyk et al. 2000; Maund et al. 2006), which are believed to be luminous non-terminal eruptions of massive stars instead of SNe. There are multiple cases of such events, e.g., the ongoing transient SN 2009ip (Pastorello et al. 2013; Fraser et al. 2013; Mauerhan et al. 2013; Prieto et al. 2013; Margutti et al. 2014; Smith et al. 2014). SN impostors are generally claimed to be LBV transients with peak luminosities lower than SNe ($M \geqslant -14$), such as SN 1997bs ($M_V \sim -13.8$; Van Dyk et al. 2000), SN 2000ch ($M_R \sim -12.8$; Wagner et al. 2004; Pastorello et al. 2010), SN 2002kg ($M_V \sim -9.6$; Weis & Bomans 2005; Maund et al. 2006; Van Dyk et al. 2006), SN 2007sv ($M_R \sim -14.2$; Tartaglia et al. 2015), SN 2008S ($M_R \sim -13.9$; Kochanek 2011; Smith et al. 2009), and 2008 NGC 300-OT ($M_V \sim -12$ to -13; Bond et al. 2009; see also the compilation paper by Smith et al. 2011). However, unambiguous evidence that all transients classified as "impostors" are actually non-terminal events is lacking. Indeed, for the first transient identified as a SN impostor, SN 1997bs, it has been claimed that no surviving star is present (Li et al. 2002; Adams & Kochanek 2015). Adams & Kochanek (2015) have argued that the scenario where the surviving star is obscured by dust created in the eruption is excluded.

Given that SN impostors and SNe IIn show similar spectroscopic features, such as the presence of narrow emission lines (in particular H I lines), differentiation based solely on spectral analysis is rendered difficult, and constraining the nature of their progenitors (e.g., ZAMS mass) has been problematic. Indeed, the detection of narrow emission lines is merely evidence for high density material close to the SN and it appears that this high density CSM can be produced by a number of different progenitor scenarios. Indeed, it has even been observed in SNe Ia (e.g., SN 2002ic, Hamuy et al. 2003; SN 2011kx, Dilday et al. 2012).

While observations of individual SNe IIn have been used to argue for LBV progenitors or LBV transients, statistical investigations of their environments within host galaxies have pointed to lower mass progenitors. Anderson et al. (2012) and Habergham et al. (2014) found a low correlation between SNe IIn and host-galaxy H II regions. It was found that SNe IIn show a degree of association with star formation (SF) similar to SNe IIP, which are thought to arise from stars at the lower end of the CC SNe scale, with masses between 8 and 16 $M_\odot$ (Smartt 2009). Therefore, these results suggest that a significant fraction of SNe IIn arise from relatively low-mass progenitors. This is somewhat surprising given that the LBV phase is thought to be associated only with very massive stars (~ 30–$80 M_\odot$). Contrary to the above, we note that recent results suggest that a significant fraction of SNe IIn could arise from electron capture SNe (Smith 2013) with AGB progenitor stars (Botticella et al. 2009; Prieto et al. 2009). Also, Smith & Tombleson (2015) argue that LBV stars are the product of binary kicks due to their isolated environments.

In this paper we present optical photometry and spectroscopy of the transient SN 2011A, originally classified as an SN IIn (Stritzinger et al. 2011). Given the properties of the transient, we discuss its characteristics in comparison to other SN IIn and SN impostors with the aim of defining the nature of the transient and constraining its properties. Due to the fact that it is unclear whether SN 2011A was a true SN, we refer to it as "transient" throughout the paper.

The paper is organized as follows. Section 2 contains a description of the observations and in Section 3 we discuss our results, first analyzing light and color curves and then using spectroscopy to derive physical parameters for the transient. In Section 4 we discuss our results and we conclude with a summary in Section 5.

2. OBSERVATIONS

2.1. Discovery

SN 2011A was discovered on an unfiltered image (apparent magnitude ~16.9) on 2011 January 2.30 UT with the 0.41 m "PROMPT 4" telescope located at Cerro Tololo (Pignata et al. 2011) on behalf of the CHASE project (Pignata et al. 2009). The transient was located at $\alpha = 13^h 01^m 01^s.19 \pm 0^s.2$, $\delta = -14°31'34''.8 \pm 0''.2$ (J2000.0), 21''.3 east and 46''.5 south of the center of the galaxy NGC 4902 at $z = 0.008916$ (Theureau et al. 2007; see NED).[13] NGC 4902 is a luminous Sb galaxy ($M_B = -21.40$). Stritzinger et al. (2011) classified the object as an SNe IIn due to the presence of prevalent narrow Balmer lines in the spectrum. The most recent pre-explosion nondetection on archival images was dated 2010 July 13.05 (limiting magnitude 18.5), providing extremely weak constraints on any explosion time or previous variability. All observations are presented with respect to the discovery date, 2011 January 2.30 UT. In Figure 1 the field of the transient is displayed.

---

[13] http://ned.ipac.caltech.edu/
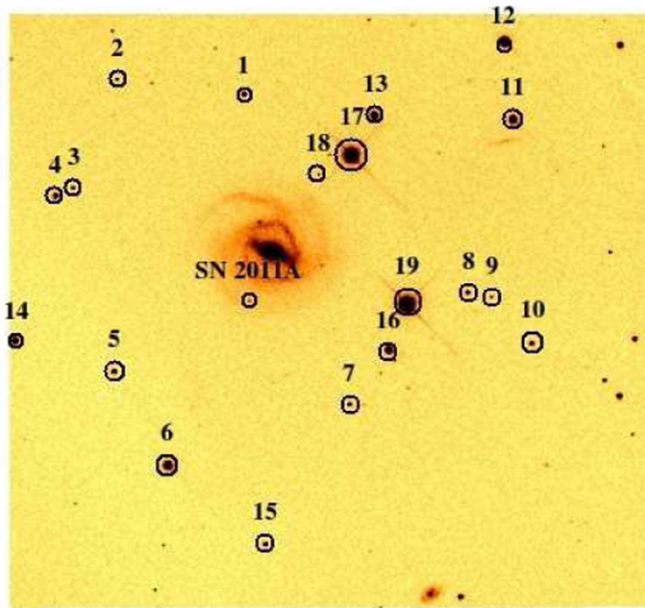
Figure 1. Field of SN 2011A showing the location of sequence stars (designated numerically) listed in Table 1. The location of SN 2011A is marked by a gray circle. North is up and east is to the left. The image is $10' \times 10'$ and was taken with PROMPT-5 on 2011 January 23 in the r' band.

2.2. Photometry

Optical photometry was obtained with the Panchromatic Robotic Optical Monitoring and Polarimetry Telescopes (PROMPT; Reichart et al. 2005) at the Cerro Tololo Inter-American Observatory, RATCam mounted on the 2.0 m Liverpool Telescope (LT; Steele et al. 2004) at the Observatorio del Roque de los Muchachos on the Canary Island of La Palma, with EFOSC2 (Buzzoni et al. 1984) mounted on the 3.6 m New Technology Telescope (NTT) at the La Silla Observatory, the 2.2 m telescope at the Calar Alto (CA) Observatory with the optical imager/spectrograph CAFOS, and from the imager AFOSC mounted at the 1.82 m reflector telescope at the Asiago Observatory. All images were analyzed after automated reductions (bias and flat-field correction and astrometric solution) had been applied and all the science images were host-galaxy subtracted.

Photometry of the transient was computed relative to a sequence of 19 stars in the field of NGC 4902, which we calibrate using catalogs from Landolt (1992, 2007) for B, V, R, I bands and Smith et al. (2002) for u', g', r', i', z' bands. Instrument-specific color terms were derived using several epochs of standard field observations. The resulting $B, V, R, I, u', g', r', i', z'$ magnitudes of the local sequence stars are reported in Table 1, which correspond to the averages from n photometric nights ($n = 2$ for the z' filter and $n \geqslant 3$ for the remaining filters), and the uncertainties are the standard deviations from the mean.

Differential photometry of the transient was done relative to the local sequence. To obtain instrumental magnitudes, we used the IRAF[14] package *SNOOPY*.[15] Photometry for SN 2011A is presented in Table 2 and the resulting light curve is displayed

---

[14] IRAF is distributed by the National Optical Astronomy Observatories, which are operated by AURA, Inc., under cooperative agreement with the National Science Foundation.
[15] SNOOPY, originally presented in Patat (1996), has been implemented in IRAF by E. Cappellaro.

in Figure 2. Errors come from the point-spread function (PSF) fit and the local sequence magnitudes.

2.3. Visual-wavelength Spectroscopy

Optical spectroscopy of SN 2011A was acquired using the GOODMAN spectrograph at the Southern Astrophysical Research (SOAR) 4.1 m Telescope, the WFCCD at the du Pont telescope located at Las Campanas Observatory (LCO), the GMOS spectrograph mounted on Gemini-North on the summit of Mauna Kea, EFOSC2 on the 3.6 m NTT at La Silla, the ALFOSC imager/spectrograph on the 2.5 m Nordic Optical Telescope (NOT) at La Palma, and IMACS mounted on the Baade telescope at LCO. In total we obtained 11 optical spectra mostly covering the optical range from $\sim$3500 to 9000 Å except for three spectra, one covering only the Hα emission and the others $\sim$4200–7000 Å. A log of the optical observations is given in Table 3.

Spectroscopic reductions were performed using standard IRAF routines. All data were debiased, flat-fielded, and cleaned of cosmic rays. Extracted one-dimensional (1D) spectra were wavelength calibrated using He–Ne–Ar/Hg–Ar/Th–Ar lamps (depending on the instrument) and the calibrations were corrected using bright night-sky emission lines. However, for the Gemini spectrum the wavelength calibration was computed before the 1D spectrum extraction. Flux calibration was determined with spectrophotometric standard stars (Hamuy et al. 1992, 1994). Atmospheric absorption features were not removed except for spectra 2.0, 64.0, and 85.9 using a telluric standard (Hamuy et al. 2006). The spectra are not corrected for Milky Way or host-galaxy extinction. The spectral sequence is shown in Figure 3.

3. RESULTS

3.1. Photometry

3.1.1. A Rare Double Plateau

One of the defining photometric features of SN 2011A, displayed in Figure 2, is the presence of a double plateau. The V-band light curve exhibits an initial plateau which lasts $\sim$15 days with a slope of $\sim$0.37 mag $\times$ 100 days^{-1}. Subsequently, the light curve declines $\sim$0.39 mag in $\sim$10 days. Then there is a second plateau phase which lasts $\sim$15 days with a slope of 0.29 mag $\times$ 100 days^{-1}, which is flatter and longer lasting at redder wavelengths. For the remaining observed epochs the light curve declines with a slope of 2.8 mag $\times$ 100 days^{-1}. If we look at the entire V-band light curve, SN 2011A declines $\sim$2.1 mag $\times$ 100 days^{-1}. To our knowledge this double plateau has only been seen previously in the transient SN 1997bs (see Section 4.1.2). Some other SNe such as SN 1993J (Richmond et al. 1994), SN 2006aj (Campana et al. 2006), or SN 2011dh (Arcavi et al. 2011) present interesting characteristics (double-humped profile) that could be similar to our double plateau, but we think that the physics is most likely distinct. Indeed the double plateau seen in SN 2011A is powered by interaction whereas the double peak (in the above events) is first due to the cooling of the shock surface material and then to radioactive decay (Nakar & Piro 2014). We note that the double plateau is not so evident in the Sloan light curves due to less well sampled photometry and noisier data. In the Landolt filters the double plateau is clearly visible in V and R, but less evident in B and I. We are confident that this is a real feature of the transient.

Table 1
B, V, R, I, u′, g′, r′, i′, z′ Local Sequence Star Magnitudes

STAR	R.A.	Decl.	B	V	R	I	u′	g′	r′	i′	z′
1	13:01:01.523	−14:28:21.35	15.78 ± 0.02	15.20 ± 0.04	14.83 ± 0.03	14.46 ± 0.05	16.65 ± 0.02	15.45 ± 0.02	15.05 ± 0.02	14.90 ± 0.04	14.91 ± 0.01
2	13:01:09.706	−14:28:07.32	17.69 ± 0.05	17.06 ± 0.04	16.69 ± 0.03	16.32 ± 0.05	18.57 ± 0.01	17.31 ± 0.03	16.91 ± 0.01	16.74 ± 0.03	16.76 ± 0.02
3	13:01:12.549	−14:29:48.59	17.20 ± 0.02	16.41 ± 0.02	15.95 ± 0.03	15.51 ± 0.04	18.35 ± 0.09	16.75 ± 0.02	16.19 ± 0.02	15.96 ± 0.03	15.94 ± 0.01
4	13:01:13.685	−14:29:56.09	15.68 ± 0.02	14.70 ± 0.03	14.12 ± 0.03	13.65 ± 0.04	17.66 ± 0.05	15.16 ± 0.04	14.38 ± 0.01	14.11 ± 0.03	14.06 ± 0.01
5	13:01:09.906	−14:32:40.66	15.96 ± 0.01	15.10 ± 0.03	14.61 ± 0.02	14.21 ± 0.41	17.60 ± 0.03	15.50 ± 0.04	14.86 ± 0.01	14.65 ± 0.03	14.65 ± 0.01
6	13:01:06.445	−14:34:08.13	13.42 ± 0.01	12.43 ± 0.03	11.87 ± 0.03	11.36 ± 0.03	15.19 ± 0.02	12.88 ± 0.04	12.14 ± 0.01	11.83 ± 0.03	11.74 ± 0.01
7	13:00:54.730	−14:33:11.10	17.33 ± 0.02	16.17 ± 0.02	15.44 ± 0.02	14.84 ± 0.04	19.52 ± 0.10	16.74 ± 0.04	15.72 ± 0.01	15.32 ± 0.03	15.19 ± 0.01
8	13:00:47.126	−14:31:26.73	16.46 ± 0.01	15.55 ± 0.02	14.98 ± 0.02	14.48 ± 0.04	18.27 ± 0.04	15.99 ± 0.03	15.23 ± 0.02	14.94 ± 0.03	14.87 ± 0.02
9	13:00:45.583	−14:31:31.08	17.99 ± 0.03	17.36 ± 0.01	17.00 ± 0.03	16.66 ± 0.04	18.72 ± 0.02	17.62 ± 0.02	17.24 ± 0.02	17.08 ± 0.05	17.08 ± 0.01
10	13:00:42.987	−14:32:14.39	16.06 ± 0.01	15.42 ± 0.03	15.03 ± 0.02	14.64 ± 0.04	16.95 ± 0.02	15.69 ± 0.02	15.26 ± 0.02	15.08 ± 0.03	15.07 ± 0.01
11	13:00:44.202	−14:28:44.77	13.21 ± 0.03	12.73 ± 0.03	12.44 ± 0.03	12.17 ± 0.04	14.21 ± 0.02	12.92 ± 0.03	12.65 ± 0.02	12.58 ± 0.03	12.64 ± 0.01
12	13:00:44.752	−14:27:31.79	12.69 ± 0.04	12.09 ± 0.03	11.72 ± 0.02	11.38 ± 0.03	13.69 ± 0.03	12.36 ± 0.01	11.94 ± 0.02	11.81 ± 0.04	11.83 ± 0.01
13	13:00:53.129	−14:28:40.67	13.90 ± 0.02	13.11 ± 0.03	12.65 ± 0.03	12.20 ± 0.04	15.15 ± 0.02	13.46 ± 0.02	12.90 ± 0.02	12.66 ± 0.03	12.61 ± 0.01
14	13:01:16.297	−14:32:11.47	14.07 ± 0.01	13.48 ± 0.03	13.15 ± 0.03	12.83 ± 0.04	14.99 ± 0.02	13.72 ± 0.02	13.37 ± 0.01	13.25 ± 0.03	13.30 ± 0.01
15	13:01:00.164	−14:35:22.03	15.98 ± 0.01	15.33 ± 0.02	14.93 ± 0.02	12.83 ± 0.04	16.74 ± 0.01	15.60 ± 0.02	15.16 ± 0.02	14.97 ± 0.03	14.96 ± 0.01
16	13:00:52.187	−14:32:20.12	13.95 ± 0.01	13.16 ± 0.02	12.70 ± 0.03	12.31 ± 0.04	15.35 ± 0.02	13.52 ± 0.02	12.94 ± 0.02	12.75 ± 0.03	12.72 ± 0.01
17	13:00:54.651	−14:29:18.73	11.16 ± 0.03	10.38 ± 0.02	⋯	⋯	⋯	10.65 ± 0.03	10.57 ± 0.04	10.39 ± 0.03	9.74 ± 0.06
18	13:00:56.730	−14:29:37.00	19.93 ± 0.05	18.61 ± 0.03	17.74 ± 0.01	17.10 ± 0.06	20.60 ± 1.56	19.19 ± 0.10	18.09 ± 0.01	17.57 ± 0.03	17.35 ± 0.02
19	13:00:51.075	−14:31:37.80	10.84 ± 0.02	10.33 ± 0.03	⋯	⋯	⋯	10.48 ± 0.06	10.58 ± 0.05	10.41 ± 0.01	9.66 ± 0.05

**Note.** Errors correspond to the standard deviation from the mean.

Table 2
Optical Photometry of SN 2011A

JD-2450000+	Epoch[a]	B	V	R	I	u'	g'	r'	i'	z'	Telescope/Instrument
5566.3	2.5	18.11 ± 0.02	17.86 ± 0.02	17.51 ± 0.02	17.38 ± 0.02	···	···	···	···	···	PROMPT/Apogee
5567.3	3.5	18.19 ± 0.04	17.86 ± 0.02	17.53 ± 0.01	17.26 ± 0.05	···	···	···	···	···	PROMPT/Apogee
5569.3	5.5	18.18 ± 0.03	17.85 ± 0.02	17.49 ± 0.04	17.40 ± 0.02	···	···	···	···	···	PROMPT/Apogee
5570.3	6.5	···	17.87 ± 0.02	17.50 ± 0.04	17.45 ± 0.02	···	···	···	···	···	PROMPT/Apogee
5573.3	9.5	18.23 ± 0.03	17.87 ± 0.02	17.54 ± 0.04	17.41 ± 0.02	···	18.05 ± 0.02	17.82 ± 0.02	17.89 ± 0.03	17.78 ± 0.09	PROMPT/Apogee
5573.6	9.8	18.23 ± 0.04	17.90 ± 0.03			···	···	···	···	···	LT/RATCam
5575.3	11.5	···	17.89 ± 0.02	17.56 ± 0.06	17.33 ± 0.04	···	···	···	···	···	PROMPT/Apogee
5575.7	11.9	18.22 ± 0.06	···	···	···	···	19.04 ± 0.08	···	···	···	LT/RATCam
5576.2	12.4	18.26 ± 0.02	17.98 ± 0.03	17.65 ± 0.04	17.41 ± 0.05	···	···	···	···	···	CA-2.2/CAFOS
5577.3	13.5	···	17.89 ± 0.02	17.56 ± 0.06	17.30 ± 0.04	···	···	···	···	···	PROMPT/Apogee
5579.6	15.8	18.22 ± 0.03	17.96 ± 0.02	···	···	18.77 ± 0.08	18.13 ± 0.03	17.92 ± 0.02	17.91 ± 0.03	18.00 ± 0.04	LT/RATCam
5581.3	17.5	18.35 ± 0.03	17.95 ± 0.02	17.57 ± 0.04	17.55 ± 0.03	···	···	···	···	···	PROMPT/Apogee
5583.3	19.5	18.50 ± 0.04	18.02 ± 0.03	17.62 ± 0.06	17.45 ± 0.05	···	···	17.97 ± 0.02	17.68 ± 0.06	···	PROMPT/Apogee
5584.3	20.5	···	18.10 ± 0.03	17.70 ± 0.04	17.51 ± 0.03	···	···	18.02 ± 0.02	18.05 ± 0.03	18.02 ± 0.05	PROMPT/Apogee
5585.7	21.9	18.41 ± 0.03	18.20 ± 0.12	17.91 ± 0.12	···	···	···	···	···	···	NTT/EFOSC2
5588.3	24.5	18.70 ± 0.04	18.24 ± 0.03	17.90 ± 0.03	17.67 ± 0.13	···	18.43 ± 0.04	18.04 ± 0.04	18.1 ± 0.080	18.42 ± 0.10	PROMPT/Apogee
5591.3	27.5	···	···	17.97 ± 0.05	17.65 ± 0.04	···	···	···	···	···	PROMPT/Apogee
5600.3	36.5	···	18.27 ± 0.02	17.98 ± 0.02	17.62 ± 0.03	···	···	···	···	···	PROMPT/Apogee
5600.7	36.9	18.81 ± 0.02	18.29 ± 0.02	···	···	19.65 ± 0.06	18.51 ± 0.02	18.20 ± 0.02	18.20 ± 0.01	18.14 ± 0.04	LT/RATCam
5602.3	38.5	···	···	···	···	···	···	18.20 ± 0.02	18.17 ± 0.02	18.15 ± 0.03	PROMPT/Apogee
5606.3	42.5	18.99 ± 0.04.	18.29 ± 0.02		···	···	···	18.24 ± 0.02	18.11 ± 0.02	18.05 ± 0.04	PROMPT/Apogee
5610.2	46.4	···	18.40 ± 0.04	18.06 ± 0.03	17.58 ± 0.05	···	···	17.98 ± 0.07	18.10 ± 0.03	18.11 ± 0.01	PROMPT/Apogee
5610.6	46.8	···	···	···	···	20.45 ± 0.20	18.80 ± 0.06	18.30 ± 0.04	18.22 ± 0.03	18.22 ± 0.05	LT/RATCam
5613.2	49.4	···	···	···	···	···	···	18.24 ± 0.06	···	···	PROMPT/Apogee
5615.3	51.5	19.39 ± 0.05	18.55 ± 0.03	18.02 ± 0.06	17.63 ± 0.03	···	···	···	···	···	PROMPT/Apogee
5615.6	51.8	···	···	···	···	···	18.96 ± 0.03	18.37 ± 0.02	18.29 ± 0.03	18.14 ± 0.03	LT/RATCam
5617.3	53.5	19.36 ± 0.04	18.55 ± 0.01	18.06 ± 0.02	17.80 ± 0.03	···	···	···	···	···	PROMPT/Apogee
5621.6	57.8	···	···	···	···	···	19.16 ± 0.02	18.50 ± 0.01	18.28 ± 0.02	18.26 ± 0.02	LT/RATCam
5623.2	59.4	19.53 ± 0.01	18.71 ± 0.05	18.08 ± 0.04	17.61 ± 0.05	···	···	18.25 ± 0.05	···	18.22 ± 0.05	PROMPT/Apogee
5633.2	69.4	···	18.94 ± 0.03	18.07 ± 0.06	17.83 ± 0.02	···	···	···	···	···	PROMPT/Apogee
5646.2	82.4	···	···	···	···	···	···	19.15 ± 0.02	18.69 ± 0.02	18.63 ± 0.04	PROMPT/Apogee
5647.1	83.3	···	···	···	···	···	20.40 ± 0.05	18.91 ± 0.04	18.80 ± 0.03	···	PROMPT/Apogee
5651.2	87.4	···	19.54 ± 0.06	···	18.44 ± 0.05	···	···	···	···	···	PROMPT/Apogee
5651.5	87.7	···	···	···	···	···	20.43 ± 0.09	19.31 ± 0.14	18.87 ± 0.33	18.85 ± 0.88	LT/RATCam
5653.1	89.3	···	19.59 ± 0.06	19.07 ± 0.02	···	···	···	···	···	···	PROMPT/Apogee
5661.4	97.6	···	20.20 ± 0.22	19.30 ± 0.11	18.79 ± 0.20	···	···	···	···	···	1.82 m Reflector/AFOSC
5666.2	102.4	···	···	···	···	···	···	19.51 ± 0.12	19.34 ± 0.10	···	PROMPT/Apogee
5677.1	113.3	···	···	19.54 ± 0.06	19.14 ± 0.05	···	···	···	···	···	PROMPT/Apogee

Note. Errors correspond to 1σ uncertainties and come from the PSF fit and the local sequence magnitudes.
[a] Days after discovery 2011 January 2.30 UT.
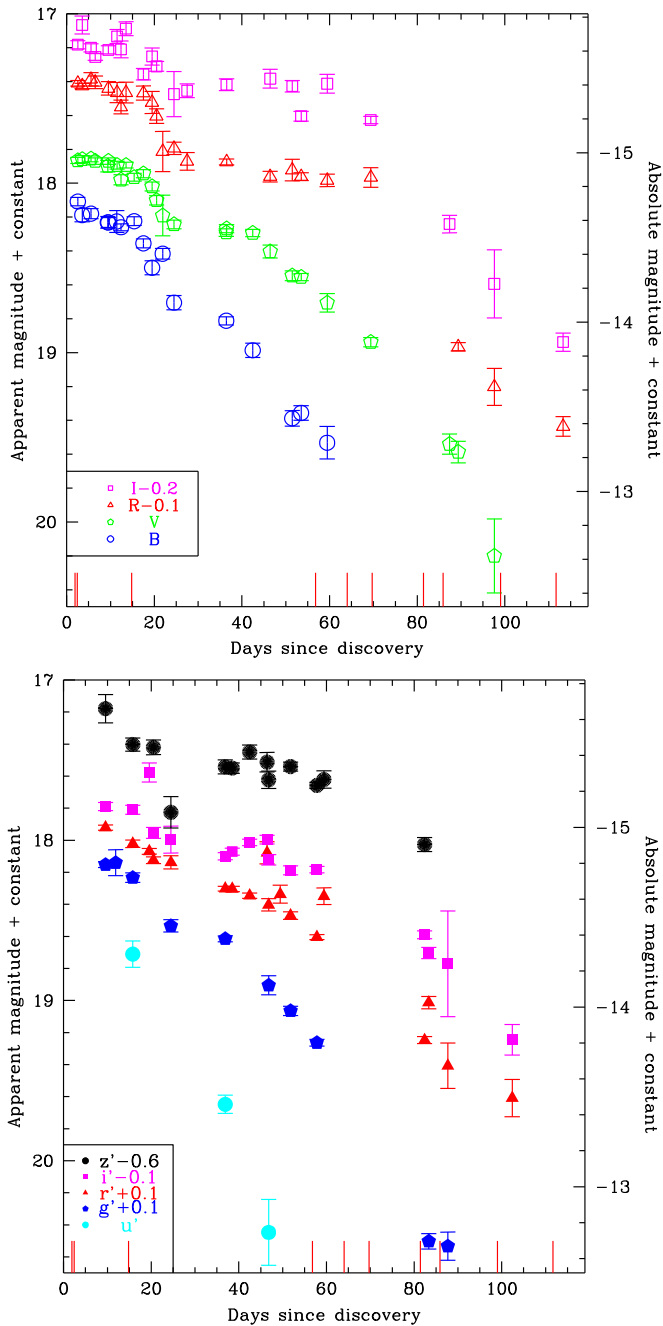
Figure 2. SN 2011A $u'Bg'VRr'Ii'z'$ band light curves. The top figure represents the light curves for Landolt filters and the bottom figure for Sloan filters. Epochs are with respect to the discovery date (2011 January 2.30 UT = 0 day). Vertical red lines represent epochs of optical spectroscopy. The apparent magnitude is shown on the left y-axis, while the absolute magnitude (calculated using only the distance modulus) is represented on the right.

3.1.2. Colors

The $(B - V)$, $(V - R)$, and $(R - I)$ color curves of SN 2011A corrected for Milky Way extinction (Schlafly & Finkbeiner 2011;[16] $A_V = 0.137$ mag and assuming $R_V = 3.1$; Cardelli et al. 1989) are presented in Figure 4. In $(B - V)$ the object shows a nearly constant color of ~0.20 mag during the first 20 days, after which it grows steadily redder until 60 days

---

[16] Via NED.

post discovery. A similar behavior is observed in $(V - R)$ except that the constant color phase of ~0.30 mag extends through day ~40 before growing redder. For $(R - I)$ we can see an increase from 0 to 0.4 mag in 100 days, but the noise prevents us from ruling out an initial phase of constant color as observed in $(B - V)$ and $(V - R)$.

3.1.3. Extinction and Absolute Magnitude

We attempt to obtain constraints on host-galaxy extinction by analyzing the early color. If we assume that the initial $(B - V) = 0.2$ mag corresponds to maximum light and that the intrinsic color was close to $(B - V) = 0.0$ mag (which is what one might expect for SNe II; see Faran et al. 2014), then $E(B - V) \sim 0.20 \pm 0.03$ mag (aware of the possibility that SNe IIn may have different colors at maximum than normal SNe II). Using $R_V = 3.1$ this implies a host-galaxy extinction $A_V \sim 0.62 \pm 0.10$ mag.

In addition we also examined the interstellar Na I D lines $\lambda\lambda 5889, 5895$ to estimate host-galaxy extinction using the spectrum with the highest resolution taken close to discovery, i.e., that obtained at Gemini-North on 2011 January 4.7 UT. The measurement of the Na I D absorption feature equivalent width (EW) yields $\mathrm{EW}(D_{1,2}) = 2.55 \pm 0.45$ Å. Unfortunately, the relation between A_V and EW for unresolved Na I D lines breaks down at EWs higher than 1 Å (Phillips et al. 2013), preventing us from deriving an independent host-galaxy extinction for SN 2011A. If this detection is due to the interstellar medium (ISM) then this would imply significant host-galaxy extinction. However, later we argue that the absorption is due to CSM material, and hence any connection with host-galaxy extinction is unclear.

Galactic extinction for SN 2011A in the V band is ~0.137 mag (Schlafly & Finkbeiner 2011)[17] assuming $R_V = 3.1$. Using a host-galaxy redshift $z = 0.008916$ (Theureau et al. 2007) and assuming a ΛCDM cosmology with $\Omega_\Lambda = 0.73$, $\Omega_M = 0.27$, and $H_0 = 73$ km s^{-1} Mpc^{-1}, we obtain a distance of 36.7 Mpc, which implies an absolute magnitude uncorrected for host extinction of $M_V = -15.10$ mag close to discovery. Aware of the uncertainties in A_V from the host galaxy $(0.62 \pm 0.10$ mag$)$, we obtain an absolute V-band magnitude of -15.72 mag. This is low for the SN IIn class $(-16 \geqslant M_V \geqslant -20$, Richardson et al. 2002), and is high compared to the SN impostors (e.g., SN 1997bs has $M_V > -14$; Van Dyk et al. 2000, or see compilation in Smith et al. 2011). It is therefore difficult to differentiate between an SN IIn or SN impostor origin for this transient using solely its M_V.

3.2. Spectroscopy

As expected for an interacting transient, the spectral sequence presented in Figure 3 is dominated by relatively narrow Hα emission. However, there is significant evolution with time, as will now be discussed.

3.2.1. Spectral Evolution

The spectrum with the highest resolution taken close to discovery (+2.4 days) is dominated by Balmer lines, most prominently Hα and Hβ in emission, with a characteristic width of ~2400 km s^{-1} measured using the FWHM. In what

---

[17] via NED.

Table 3
Log of Optical Spectroscopy of SN 2011A

JD −2450000+	UT Date	Epoch[a]	Telescope/Instrument	Exposure (s)	Grating	Resolution FWHM (Å)	Resolution (km s^{-1})	Range (Å)
5565.8	Jan 4.3	2.0	du Pont/WFCCD WF4K-1	600	Blue Grism	8.0	365	3630–9100
5566.2	Jan 4.7	2.4	Gemini-North/GMOS	2 × 600	B600+G5307	5.2	240	3580–9100
5578.7	Jan 17.2	14.9	NOT/ALFOSC	3 × 1200	Grism 17	1.5	70	6330–6900
5620.6	Feb 28.1	56.8	SOAR/GOODMAN	2 × 1200	RALC 300	14	640	4200–8800
5627.8	Mar 7.3	64.0	du Pont/WFCCD	1000	Blue Grism	8.0	365	3700–9180
5633.8	Mar 13.3	70.0	SOAR/GOODMAN	2 × 2700	KOSI 600	5.1	235	4380–7015
5644.7	Mar 24.2	80.9	NTT/EFOSC2	2 × 3600	Grism 11/16	14.0	640	3740–9000
5649.7	Mar 29.2	85.9	Baade/IMACS	4 × 2000	300-4.3 Grating	2.7	120	4190–9000
5662.3	Apr 10.8	98.5	NTT/EFOSC2	2 × 3600	Grism 11/16	14.0	640	3610–9050
5675.6	Apr 24.1	111.8	SOAR/GOODMAN	2 × 2700	KOSI 600	7.0	320	4350–7015
5708.5	May 27.0	144.7	SOAR/GOODMAN	2 × 2400	RALC 300	10.2	470	3650–8840

Note.
[a] Days after discovery 2011 January 2.30 UT.
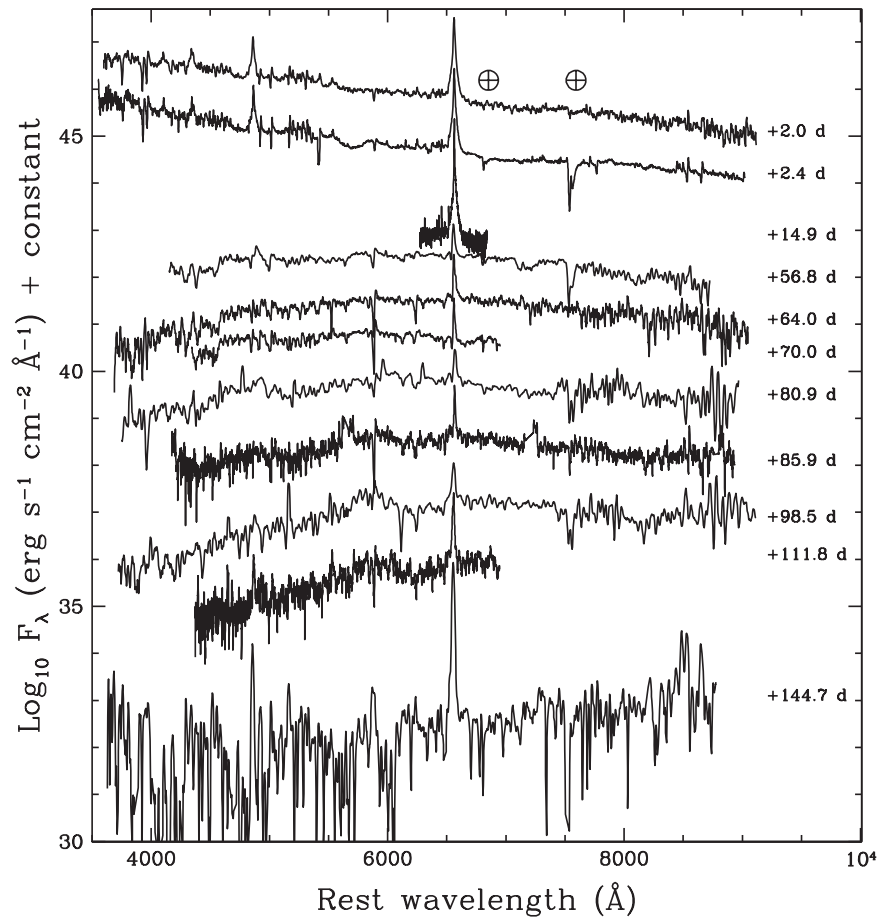
Figure 3. Optical spectra of SN 2011A taken with the SOAR, NTT, Gemini-North, NOT, Baade, and du Pont telescopes. The epochs post discovery (2011 January 2.30 UT) are listed. Atmospheric absorption features were not removed except for spectra at 2.0, 64.0, and 85.9 days, and are indicated with a ⊕ symbol. Spectra were smoothed using a boxcar of 5 pixel size. The flux calibration of the spectra was revised using multi-color photometry. The spectra have not been corrected for Milky Way or host-galaxy extinction.

follows we will refer to these lines as "broad," although the reader should keep in mind that these velocities are much lower than what is observed in most SNe II ($v \sim 10^4$ km s^{-1}). We also observe many narrow ($\sim$500–1000 km s^{-1}) P Cygni profiles attributed to Ca II $\lambda\lambda$3933, 3968, the Ca II near-infrared

triplet $\lambda\lambda$8498, 8542, 8662, and many Fe II lines. After $\sim$day 50, Hα emission is still present but Hβ is significantly weaker. We see a similar evolution of the Fe II lines, which are present during the first few days but disappear from day 56.8 onward. The Ca II triplet is not clearly seen in spectra between days 56.8
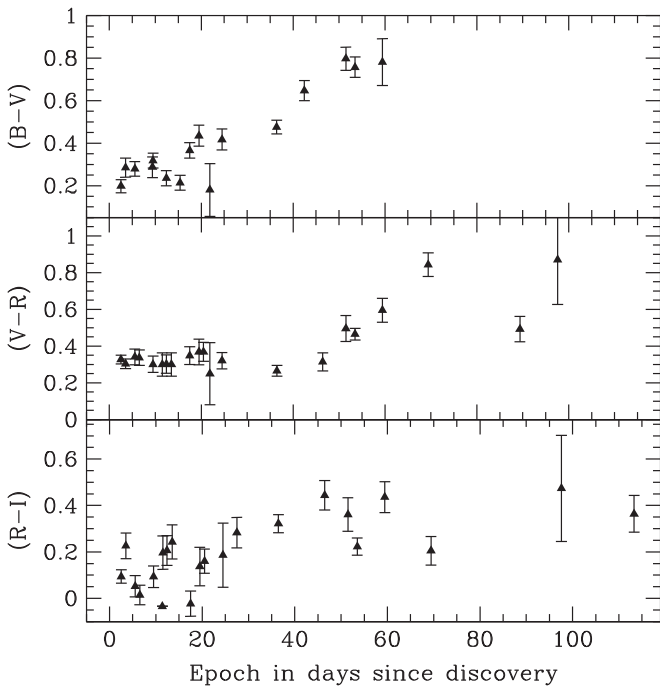
**Figure 4.** Observed $(B - V)$, $(V - R)$, $(R - I)$ color evolution of SN 2011A corrected for Milky Way extinction.
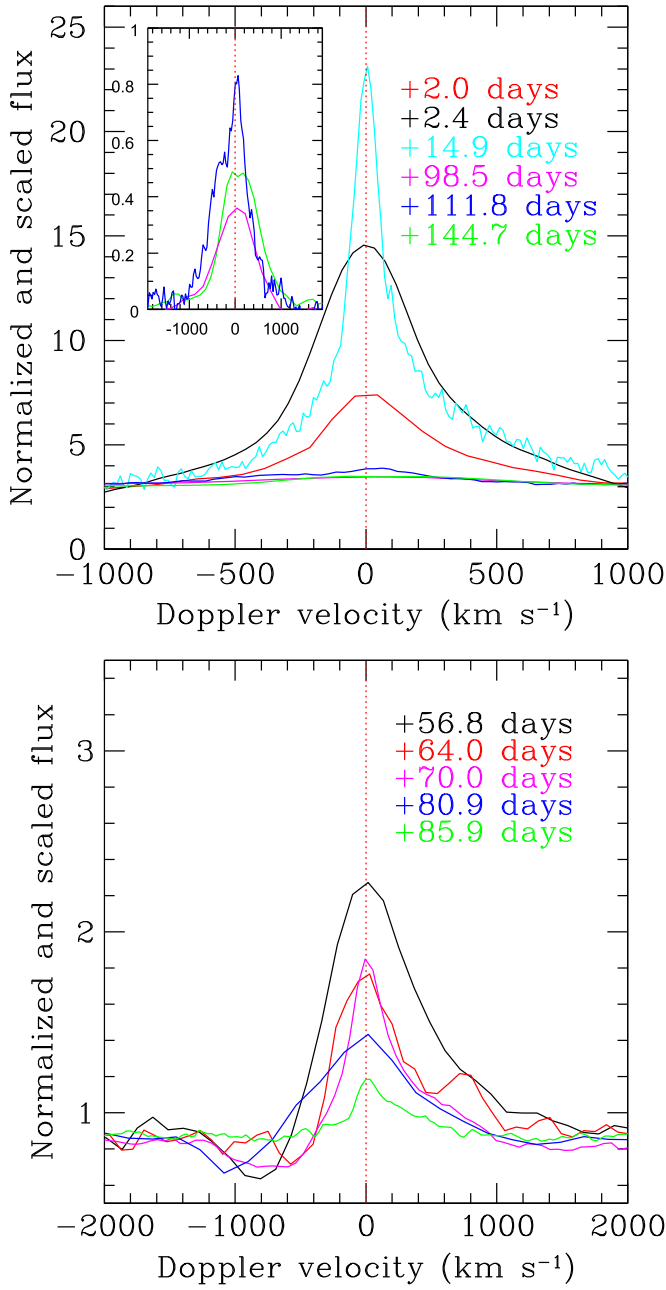

Figure 5. Hα line profile evolution of SN 2011A. The epochs are indicated in black and are with respect to the discovery date (2011 January 2.30 UT = 0 days). The dotted red vertical line represents the rest-frame Hα wavelength at 6562.81 Å.

and 85.9 due to noisy data but is still visible on the +98.5 day spectrum, and possibly 144.7 days after discovery.

To understand SNe IIn, it is common practice to analyze the Hα line profile and its evolution. This is shown in Figure 5 where we see considerable temporal variations. Indeed, from discovery to 56.8 days later, our spectra are characterized by prominent "broad" emission ($v \sim 2000 \, \mathrm{km \, s^{-1}}$). Then between 56.8 and 85.9 days post discovery, narrow low-velocity (600–1100 $\mathrm{km \, s^{-1}}$) P Cygni absorption appears. After day 85.9 we see again a "broad" emission with no signs of the P Cygni profile. Again, we emphasize the absence in the spectra at all epochs of any kind of high-velocity component ($\sim 10^4$ $\mathrm{km \, s^{-1}}$) characteristic of SN ejecta.

In Figure 6 we show the Hα line evolution splitting it into epochs with and without P Cygni profiles. The P Cygni component is seen in spectra obtained on days +56.8, +64.0, +70.0, and +80.9. The blueshifted absorption velocity has values between 575 and 1060 $\mathrm{km \, s^{-1}}$. It is unlikely that these low-velocity P Cygni profiles can be attributed to the ejecta, which is expected to have velocities of several thousand $\mathrm{km \, s^{-1}}$. Therefore, we argue that this P Cygni component is related to a pre-SN wind. The wind velocity is consistent with an LBV progenitor (100–1000 $\mathrm{km \, s^{-1}}$; Smith & Townsend 2007) but is too high for red supergiants (20–40 $\mathrm{km \, s^{-1}}$; Smith et al. 2007) and possibly too low for Wolf–Rayet stars (1000–5000 $\mathrm{km \, s^{-1}}$; Abbott & Conti 1987).

Our first spectra, taken 2.0 and 2.4 days after discovery, show many strong Fe II features with P Cygni profiles. The velocity measured with respect to the emission from the Fe II multiplet $\lambda\lambda 4923, 5018, 5169$ lines in the +2.4 day spectrum is between 430 and 460 $\mathrm{km \, s^{-1}}$, arguing for a CSM rather than ejecta origin. We also note that these velocities have the same order of magnitude as those derived from the Hα P Cygni
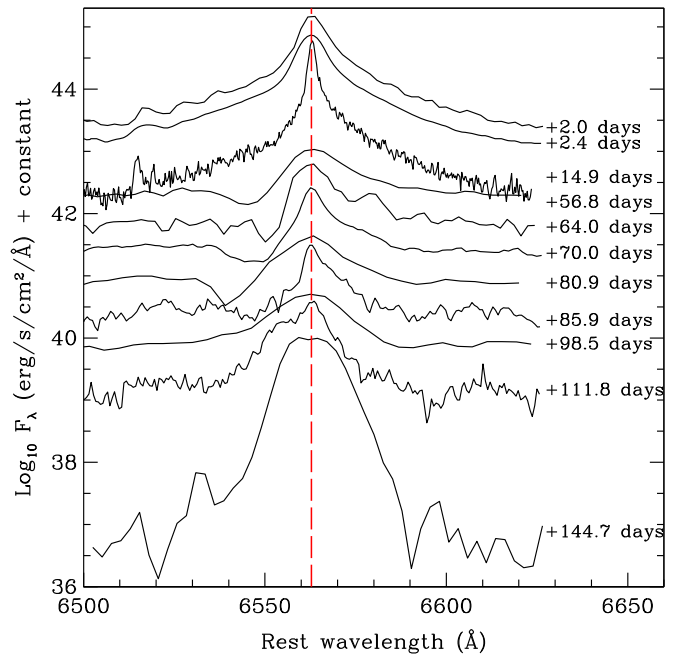
component. The same is seen in the red part with the calcium triplet $\lambda\lambda 8498, 8542, 8662$. Indeed in the +2.4 day spectrum we measured low velocity with respect to the emission ($\sim 440 \, \mathrm{km \, s^{-1}}$), again supporting the hypothesis of a CSM origin and consistent with the velocities derived from the Fe II lines. Looking at the continuum we can also estimate the temperature through a blackbody fit. The temperature evolution shows a rapid decline from ≈ 9000 K in the +2.0 day spectrum to ≈ 5000 K in the +56.8 day spectrum and to ≈ 3300 K at later epochs.

3.2.2. Variable Low-velocity Absorption Close to Na I D

As seen in the Type IIn SN 1994 W (Chugai et al. 2004), we observe strong absorption near the Na I D doublet wavelength ($\lambda\lambda 5889, 5895$) that becomes stronger with time and has low velocity. This is shown in Figure 7, where the evolution of this feature is presented. The EW and velocity of the line profile were calculated for each epoch. Because the majority of our spectra were taken in low resolution, the sodium doublet is unresolved; hence, we will refer to this feature as absorption at the wavelength of Na I D due to the fact that the Na I D can be blended with the He I $\lambda 5876$ line (we also note the possible presence of He I at the wavelengths $\lambda 6678$ and $\lambda 7065$ in the 2.4 day spectrum). Therefore the total blended doublet is measured as a single line. In Figure 8 we present both the EW and velocity evolution and see that the absorption becomes stronger with time. Indeed the EW is initially equal to ~ 3 Å and increases to 10 Å after the first 70.0 days. At the same time, the feature profile evolves. In the first two spectra, only an absorption line is observed, while between days 56.8 and 110.3 a P Cygni profile appears. The velocities are measured from the Na I D center, 5892 Å, with respect to the emission are shown in Table 4. Figure 8 also

Figure 7. Zoom on the absorption near Na I D of our SN 2011A optical spectra. The epochs are listed with respect to the discovery date (2011 January 2.30 UT = 0 days). The red line represents the center of the Na I D corrected to the redshift of the host galaxy. We note that this appears offset by ~200 km s^{-1} from the emission component of Na I D.

Figure 6. Hα line profile evolution. The top figure shows the Hα line profile showing a broad component without absorption. We also present a zoom on Hα for late spectra. The bottom figure shows the Hα line profile with P Cygni absorption. We normalized all spectra with respect to the Gemini spectrum continuum. The scale has been adjusted to overlap the broad wings of Hα.

Figure 8. Top: the absorption near the Na I D equivalent width evolution with time for SN 2011A. The solid blue line shows the average Na I D EWs (averaged over time) for all CSP SNe II (including SNe IIn, but not SNe IIb) where the EW is most likely of ISM origin. The lower dashed blue line shows the 1σ error on the EW estimation, and the upper shows the 3σ error. The lower panel shows the absorption near the Na I D velocity evolution measured with respect to the emission.

3.2.3. Wind Velocity

In order to measure the wind velocity we estimate the width of the narrow component of the Hα emission line. For this

shows the average Na I D EWs from the ISM for all of the Carnegie Supernova Project (CSP; Hamuy et al. 2006) SNe II (as used in Anderson et al. 2014b). We measure the EW for each SN regardless of the epoch and we averaged these values. This is again further evidence of a CSM origin for this line: the strength is much higher than seen in any other SNe II from the CSP database. Even if the low-resolution spectra prevent us from being sure that the measured absorption close to Na I D position is only due to Na I D and not blending with other lines, the absorption strength is unprecedented.

Table 4
Evolution of the Absorption Near Na I D with Time

Epoch[a]	Equivalent Width (Å)[b]	Velocity (km s^{-1})[b]	Line Profile
2.0	3.2(0.5)	530(25)	absorption
2.4	2.6(0.7)	400(30)	absorption
56.8	6.9(0.35)	500(75)	P Cygni
64.0	11.5(0.7)	510(55)	P Cygni
70.0	9.5(0.3)	490(70)	P Cygni
80.9	8.0(1.1)	820(50)	P Cygni
85.9	10.8(0.5)	600(75)	P Cygni
98.5	7.7(0.8)	830(125)	P Cygni
111.8	10.6(1.6)	400(130)	P Cygni
144.7	…	…	…

Note.
[a] Days after discovery on 2011 January 2.30 UT.
[b] We note in parenthesis the associated error. The errors come from the uncertainties of defining the continuum for measurement of the absorption and emission components. This was achieved using multiple measurements, changing the continuum position each time. The velocities are measured from the Na I D center, 5892 Å, with respect to the emission.

estimation we decompose the Hα feature using a least-squares PYTHON script, which solves the best-fit multi Gaussian decomposition. The best fit was performed using three components, so nine parameters are used as input: the FWHM, the amplitude, and the center of each Gaussian corresponding to the three components. Using these values our script provides the best-fit Gaussian parameters, the best FWHM, the amplitude, and the center of each component. The errors on these parameters are derived assuming a reduced chi squared equal to one. In Figure 9 we show the Hα emission line decomposition for spectra taken with ALFOSC (highest resolution spectrum available) on 2011 January 17.2 UT. Our three components fit to the Hα emission line yield velocities of 107 ± 2, 467 ± 14, and 1971 ± 35 km s^{-1}. Each velocity component is low compared to other SNe IIn. For comparison, Kiewe et al. (2012) found typical velocities of 2000 km s^{-1} for the intermediate component. We also note that Pastorello et al. (2004) found that for low-luminosity SNe II the expansion velocities range from 3000 to 5000 km s^{-1} during early epochs. Therefore, SN 2011A appears to have ejecta velocities lower than the majority of normal SNe events. This could be evidence for an SN impostor origin, as will be discussed below. In addition, Tartaglia et al. (2015) recently reported a case of an interesting transient, SN 2007sv. From this object the authors, also analyzing the Hα emission line, derived very similar velocity values. Indeed the broad component velocity was estimated as 2000 km s^{-1} (1971 km s^{-1} for SN 2011A), the intermediate component velocity as 600–800 km s^{-1} (467 km s^{-1} for SN 2011A), and the narrow component velocity as 120–150 km s^{-1} (107 km s^{-1} for SN 2011A). In their paper, they conclude that the transient SN 2007sv is most likely an SN impostor, based mainly on its absolute magnitude. Note that the absolute magnitude derived for this transient is ~2 mag fainter than SN 2011A.

Note that from the Gaussian decomposition of the highest resolution spectrum we can calculate the progenitor mass-loss rate using the following formula (Chugai & Danziger 1994;
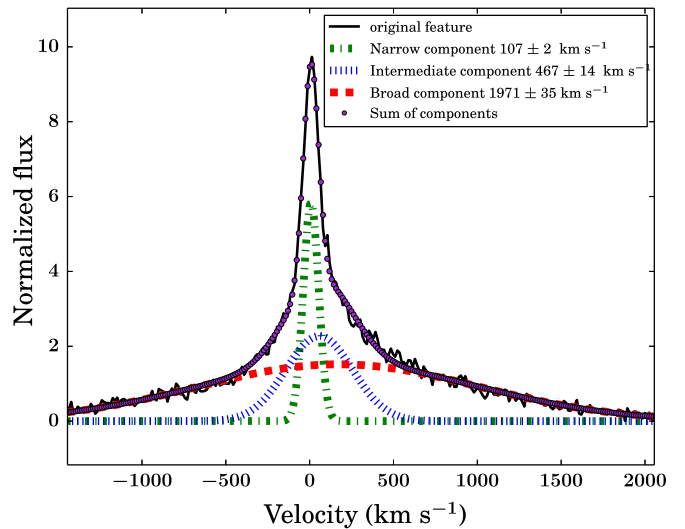
Figure 9. Decomposition of the Hα emission line for the spectrum taken with ALFOSC at NOT on 2011 January 17.2 UT.

Kiewe et al. 2012):

$$L_{H_\alpha} = \frac{1}{2}\dot{M}\psi\frac{v_{shock}^3}{v_{wind}} \qquad (1)$$

where ψ is the efficiency of the conversion of mechanical energy into optical energy in the shock wave (we adopt as Kiewe et al. 2012, $\psi = 0.1$), $\dot{M}$ is the mass-loss rate, v_{wind} is the unshocked wind velocity derived as described above, and v_{shock} is the shock velocity. The shock velocity was taken as the FHWM of the intermediate width component. The absolute L_{H_α} was then obtained by integrating over the intermediate width feature and taking account of the distance to the SN. We used the same luminosity distance used above, i.e., 36.70 Mpc. We found $\dot{M} = 0.038\ M_\odot$ yr^{-1} with a wind velocity of 110 km s^{-1} and a shock velocity about 470 km s^{-1}. This mass-loss rate is consistent with values found by Kiewe et al. (2012) and is too high for any class of massive stars other than LBVs in the eruptive phase (Humphreys & Davidson 1994).

4. DISCUSSION

SN 2011A shows a number of interesting properties. In order to understand the nature of the transient, we compare in this section our object with other interacting transients. We discuss the transient in comparison to other events that possibly show similarities. However, in any case where similarities exist, we show that there are other features that confirm the uniqueness of SN 2011A.

4.1. Photometry

4.1.1. Photometric Comparison to other SNe IIn

As stated in the Introduction, the SN IIn group is very heterogeneous in terms of luminosity, light curve shape, and spectral evolution. Based on Kiewe et al. (2012), who proposed to differentiate SNe IIn according to their photometric and spectroscopic characteristics, Kankare et al. (2012)
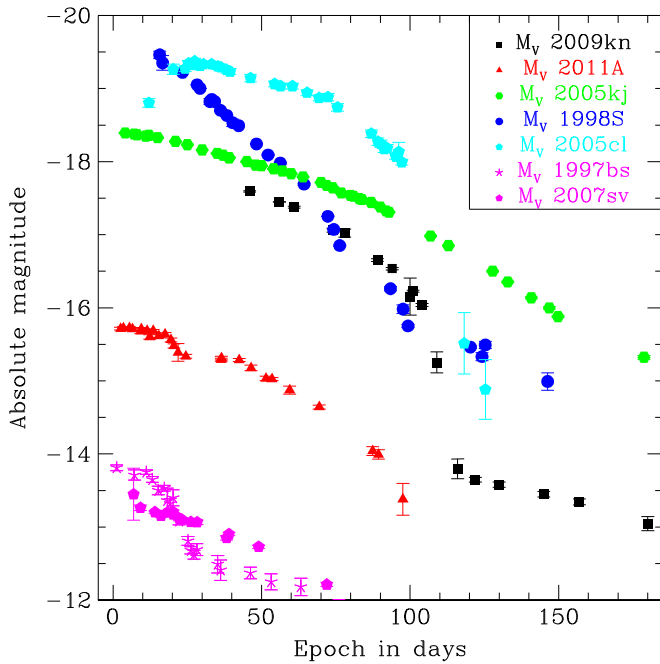
Figure 10. Comparison of the absolute V-band light curves of SN 2011A, SN 1998S (Fassia et al. 2001), SN 2009kn (Kankare et al. 2012), SN 2005cl (Kiewe et al. 2012), SN 2005kj (Taddia et al. 2013), SN 1997bs (Van Dyk et al. 2000), and SN 2007sv (Tartaglia et al. 2015). Each SN was corrected for Milky Way extinction. Full red triangles represent SN 2011A corrected for host-galaxy extinction ($A_v = 0.62$ mag). For SN 2009kn we use the explosion date estimation from Kankare et al. (2012). For SN 1998S, SN 2005kj, SN 2005cl, SN 1997bs, and SN 2007sv we use the discovery date as the explosion date. For each SN we applied the host-galaxy extinction estimated by the authors.

Figure 11. $(B - V)$, $(V - R)$, $(R - I)$ color evolution of SN 2011A (red triangles) compared to other SNe, SN 2009kn (Kankare et al. 2012) shown in black squares and SN 1998S (Fassia et al. 2000) represented by blue circles. All colors were corrected for Milky Way extinction and by host-galaxy extinction. For SN 2011A and SN 1998S the epochs are with respect to the discovery date, whereas for SN 2009kn they are with respect to the explosion date estimated by the authors.

identify a subclass of SNe IIn in which they included SN 2009kn (Kankare et al. 2012), SN 1994W (Chugai et al. 2004), and SN 2005cl (Kiewe et al. 2012). To see if SN 2011A shares common properties with these SNe and belongs to this subclass, we compare the light curves and spectra (see Section 4.2.2). We also include a comparison with SN 1998S (Fassia et al. 2001), a well studied SN IIn, SN 2005kj (Taddia et al. 2013), which, similar to SN 2011A, shows evidence of low-velocity absorption at Na I D wavelengths, SN 1997bs (Van Dyk et al. 2000) classified as an SN impostor (note that we compare SN 2011A and SN 1997bs in more detail in Section 4.1.2), and SN 2007sv, also recently classified as an SN impostor (Tartaglia et al. 2015). These comparisons are shown in Figure 10, where the V-band light curves are plotted. Note that we do not present the SN 1994W light curve due to the lack of data and because it is very similar to SN 2009kn (Kankare et a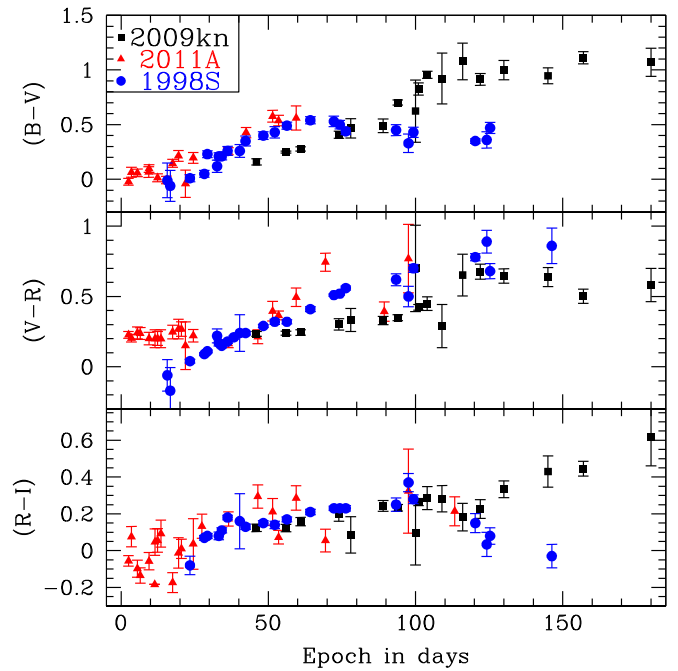l. 2012). As we can see in Figure 10, SN 2009kn is brighter than SN 2011A with $M_V \simeq -17.5/-18$ and the SN 2009kn light curve does not show a double plateau like SN 2011A. Indeed, after an initially declining plateau phase with a slope equal to 0.018 mag day^{-1}, we see a quick fall around 0.08 mag day^{-1} followed by a slow decline phase with a slope of ~ 1 mag 100 day^{-1}. However, the photometry of SN 2009kn does not cover the first few tens of days from the assumed explosion date. As can be seen in Figure 10, SN 2011A is photometrically very different that other SNe IIn. None of the other selected SNe IIn show a double plateau and they are all $\geqslant 2$ mag brighter than SN 2011A. Also we remark that SN 2011A is ~ 2 mag brighter than the SN impostors. Figure 10 allows us to conclude that SN 2011A

is a very rare event that does not share any similarities in the light curve with other SN 1994W-like SNe IIn. An important additional point to note is the origin of the two SNe IIn, SN 1994W and SN 2009kn, used to compare SN 2011A to other SNe IIn. Indeed the origin is not so clear; for example Dessart et al. (2009) argued that maybe SN 1994W was not an SN, but rather the result of two interacting shells of material related to LBV-like eruptions. Also, in the case of SN 2009kn (Kankare et al. 2012) a non-SN origin could not be completely excluded, but also found the observations to be consistent with an electron capture SN. We note that an argument will be presented later that constrains the epoch of the photometry of SN 2011A to be ~ 50 days later than shown in Figure 10. However, the main conclusions remain valid: SN 2011A has a luminosity between the two classes of interacting transients, SNe IIn and SN impostors; this event shows a rare double plateau.

In Figure 11 we present the optical colors of SN 2011A together with the color evolution of SN 2009kn, one SN 1994W-like, and the well studied SN 1998S. We do not present the SN 1994W and SN 2005cl colors due to the lack of data. All magnitudes were corrected for Milky Way extinction. Taking the discovery date as the explosion date, the color evolution of SN 2011A looks fairly similar to SN 1998S. Indeed, the $(B - V)$ color becomes redder in SN 1998S between days 0 and 60. However, in $(V - R)$, SN 1998S does not show an initial plateau as in SN 2011A.

The color evolution of SN 2009kn looks similar to SN 2011A in $(B - V)$ and $(V - R)$, but shifted by ~ 50 days. This could be explained by the lack of precision in the explosion date for SN 2011A. If we shift our epochs by 50 days (motivated by the spectral analysis in Section 4.2.1), the color

Figure 12. Comparison of the *BVRI* light curves of SN 2011A and the impostor SN 1997bs. Photometric data of the SN impostor were taken from Van Dyk et al. (2000). For each band, empty symbols represent SN 2011A and filled symbols SN 1997bs. Squares represent the *I*-band light curve, triangles the *R*-band, hexagons the V-band and circles the *B*-band.
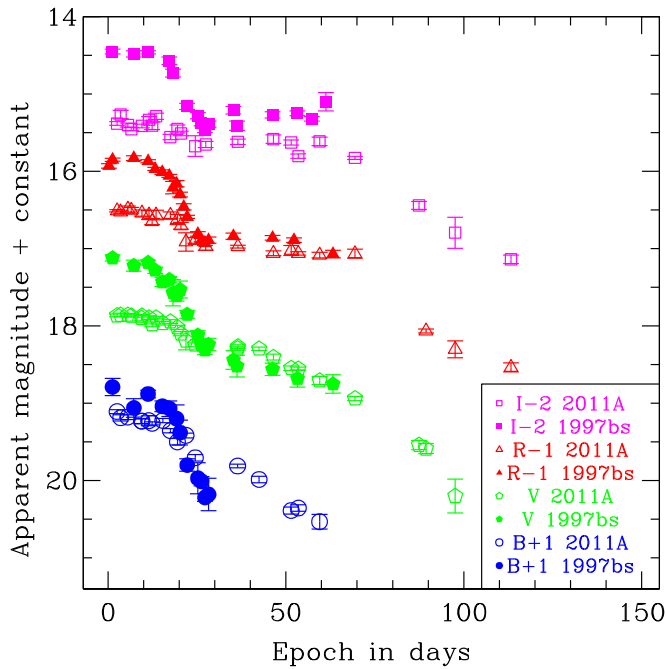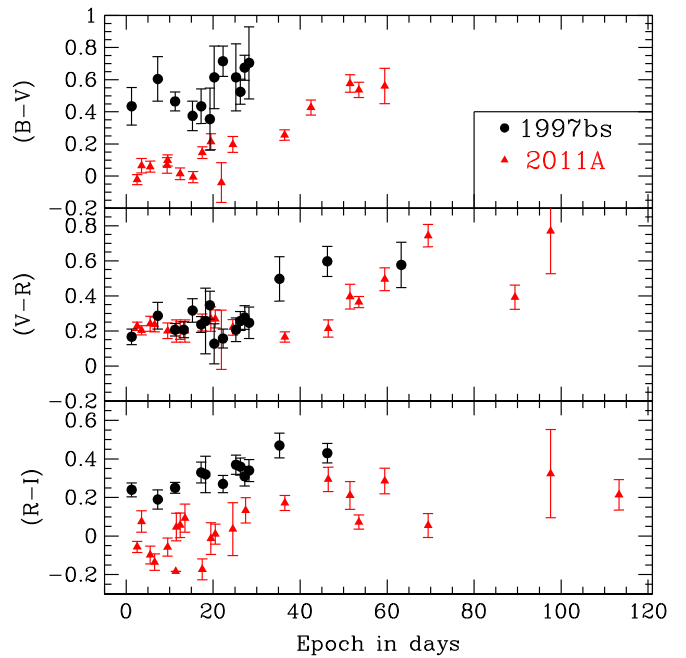

Figure 13. $(B-V)$, $(V-R)$, $(R-I)$ color evolution of SN 2011A (red triangles) compared to the impostor SN 1997bs (Van Dyk et al. 2000) shown in black circles. All colors were corrected for Milky Way extinction and by host-galaxy extinction.

evolution in $(B-V)$ and $(V-R)$ is very similar to SN 2009kn. Indeed for $(V-R)$, SN 2009kn shows a small plateau during $\sim$50 days and then an increase from 0.3 to 0.7 mag. It is more difficult to compare the behavior of the $(R-I)$ color due to their larger errors; however, we can see the same trend: for SN 2011A, $(R-I)$ increases from $\sim$0 to $\sim$0.4 mag in 100 days, and for SN 2009kn, $(R-I)$ increases from $\sim$0.2 to $\sim$0.55 mag in the same temporal windows. The colors between SN 2011A and SN 2009kn are very similar, but shifted by 50 days, which could be consistent with the hypothesis proposed in Section 4.2.1, namely, that the explosion date is not close to the discovery date but more consistent with being 50 days earlier.

4.1.2. SN 2011A versus SN 1997bs

The light curve comparison between SN 2011A and SN 1997bs (which was classified as an SN impostor by Van Dyk et al. 2000) shows similarities. The light curves of both objects in *B*, *V*, *R*, and *I* bands are shown in Figure 12. For the SN 1997bs explosion date, we chose 1997 April 15th (UT discovery date), which should be valid because an image taken on 1997 April 10th does not show anything at the location of the SN. During the first 15 days of evolution in the *R* and *I* bands both objects exhibit a plateau. After this first plateau the two transients show a second plateau but the drop between the two is much larger for SN 1997bs: $\sim$0.5 mag for SN 2011A and $\sim$1 mag for SN 1997bs in *R*. The *B* and *V* bands have also some similarities. Note that while the light curve evolution displayed in Figure 12 appears to be very similar, this may be coincidental given the uncertainty of the SN 2011A explosion date. However, the important observation is the similar double plateau features in both light curves, which may be evidence for the same underlying mechanism, namely,

interaction with two separate CSM shells. The optical colors of SN 2011A compared with SN 1997bs are presented in Figure 13. From the $(B-V)$ color we can compare the colors near maximum. For SN 2011A we find $\sim$0.25 mag whereas for SN 1997bs Van Dyk et al. (2000) found 0.67 mag, adding host extinction for 1997bs. Additionally we can compare the color evolution. In the $(V-R)$ color, the evolution looks similar during the first 30 days. For SN 1997bs, a plateau at 0.3 mag for 30 days is seen and then reddening as for SN 2011A. However, in SN 2011A the plateau lasts 50 days. Despite the noise, the $(B-V)$ color exhibits the same trend with a plateau for 20 days and then reddening. Again, in $(R-I)$, SN 2011A and the SN impostor show the same evolution with reddening during the first 40 days. Although the data are noisy, the shape of the reddening is pretty similar. Finally, note that the SN impostor nature of SN 1997bs is not entirely clear, as there is some evidence that the progenitor did not survive until the explosion (Li et al. 2002; Adams & Kochanek 2015). Hence, while SN 2011A shows similarities to SN 1997bs, this is not conclusive proof that the former was an imposter event.

4.1.3. ^{56}Ni Mass Estimate

One diagnostic to discriminate between SNe and SN impostors is the amount of synthesized ^{56}Ni. For low-mass core-collapse SNe (SNe IIP) one expects to find a ^{56}Ni mass around 0.0016–$0.26\,M_{\odot}$ (Hamuy 2003) whereas for non-terminal explosions we do not expect any ^{56}Ni production because only the outer layers of the star are ejected. For very massive CC SNe produced by progenitors with initial masses between 30 and 100 $M_{\odot}$, ^{56}Ni masses between 2.3 and 6.6 $M_{\odot}$ have been predicted (Umeda & Nomoto 2008), and masses between 0.07 and 0.6 $M_{\odot}$ have been estimated for progenitor masses between 16 and 46 $M_{\odot}$ (Mazzali et al. 2009). We can obtain a ^{56}Ni mass estimate using the formula from Hamuy
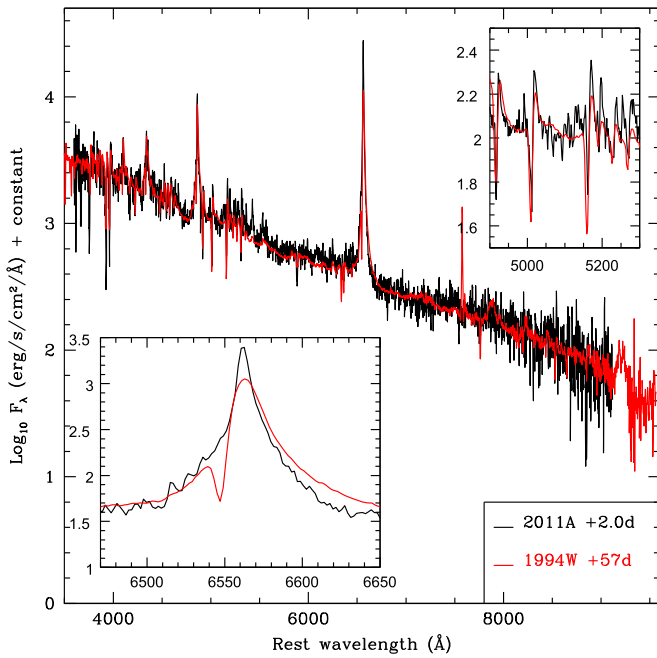
Figure 14. Comparison between the SN 2011A spectrum taken 2.0 days after discovery, in black, and that of SN 1994 W taken +57 days after explosion, in red. In the top right inset we zoom on the Fe II lines, $\lambda\lambda 4923, 5018, 5169$. In the bottom left inset we zoom on the Hα emission line. For both spectra we did not apply any MW or host-galaxy extinction correction.

Figure 15. Comparison between the SN 2011A spectrum taken 2.0 days after discovery, in black, and that of SN 1997bs taken on April 16th, one day after discovery, in red (no detection on 1997 April 10th). In the top right inset we zoom on the Fe II lines, $\lambda\lambda 4923, 5018, 5169$. In the bottom left inset we zoom on the Hα emission line. We applied a total reddening of $E(B-V) = 0.24$ mag to SN 1997bs in order to match the continua.

(2003) and the last V-band magnitude (epoch 97.6 days). This value should be taken as an upper limit of the ^{56}Ni mass because the spectrum at this epoch does not indicate that the emission is being solely powered by radioactivity. Indeed, in this spectrum narrow lines are still present due to interaction.

As stated previously the explosion date is not well constrained and could be 50 days before discovery. Therefore, the ^{56}Ni mass is calculated assuming the explosion date as the discovery date and also using an explosion date 50 days before discovery. We find 0.01–$0.015\,M_\odot$ without extinction and 0.03–$0.05\,M_\od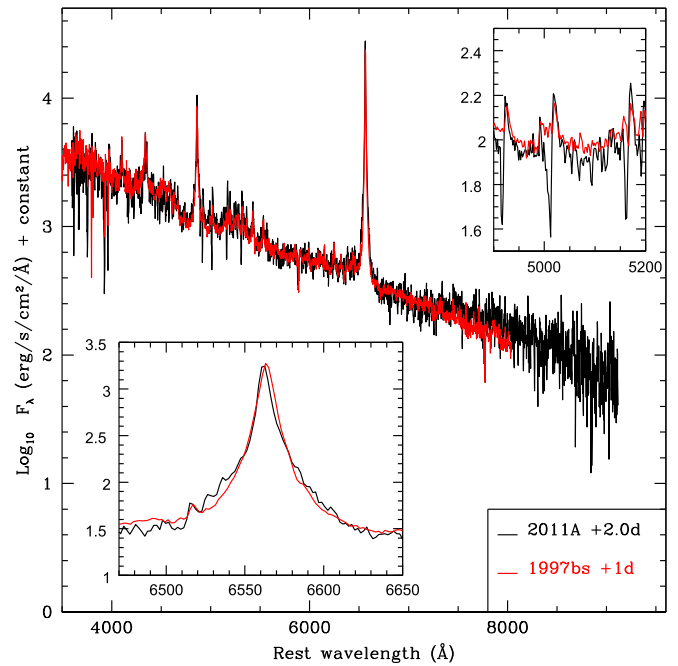ot$ with extinction. In both cases we use an explosion date 50 days before discovery for the upper value. These values are consistent with Hamuy (2003) and lower than Mazzali et al. (2009). Indeed, Hamuy (2003) found SNe II values between 0.0016 and $0.26\,M_\odot$ and Mazzali et al. values between 0.07 and $0.6\,M_\odot$. If we apply this same approach to SN 1997bs, we find a ^{56}Ni of $0.003\,M_\odot$ based on the V-band magnitude measured 63.5 days after discovery. In conclusion, it is very difficult to set significant constraints on the nature of SN 2011A based on these uncertain ^{56}Ni mass estimates.

4.2. Spectroscopy

4.2.1. Explosion Date

Unfortunately, the explosion date of SN 2011A is not well determined by pre-explosion images. A fit to the early time spectrum with a blackbody function yields a high temperature ($\sim$10,000 K), thus suggesting that the observations possibly began soon after explosion. However, given the interacting nature of SN 2011A, the validity of such a constraint is unclear. To better estimate this parameter, we compare SN 2011A with two other SNe with well constrained explosion times.

First, we consider SN 1994W (Cortini et al. 1994), for which Sollerman et al. (1998) estimated from its R-band data a precise

explosion date of 1994 July 14^{+2}_{-4}. In Figure 14 we compare our spectrum taken 2.0 days after discovery with an SN 1994W spectrum taken 57 days after explosion. As we can see, the spectra are remarkably similar. A blue continuum characterizes both spectra and the slope/shape are nearly identical. Also, both SNe show strong Fe II multiplet $\lambda\lambda 4923, 5018, 5169$ lines with low-velocity ($\sim$hundreds of km s^{-1}) P Cygni profiles (Figure 14, top right). We also distinguish in the blue part of the spectrum strong absorption attributed to Ca II $\lambda\lambda 3933, 3968$. SN 2011A shows two noticeable differences from SN 1994W: (1) the Ca II near-infrared triplet is more prominent than in SN 1994 W and (2) SN 1994 W shows a narrow P Cygni absorption on top of the broad of Hα component, whereas in SN 2011A this feature is not seen and only appears in the spectrum taken +56.8 days after discovery.

Second, in Figure 15 we compare our +2.0 day spectrum with the SN 1997bs spectrum taken on 1997 April 16th (day +1 after discovery) to search for similarities in their light curves. Given that the nondetection was very close to discovery, the explosion date is well constrained for SN 1997bs. The continua look very similar when we apply a total reddening of $E(B-V) = 0.24$ mag to SN 1997bs (Van Dyk et al. 2000 estimated this total color excess at 0.21 mag) and null for SN 2011A. We chose this color excess value to match the two continua. The spectra show some differences, most notably the lack of narrow P Cygni Fe II lines in SN 1997bs. In contrast, their Hα emission profiles are virtually identical. Note also that if these spectra were taken at similar epochs then this would imply that the host-galaxy extinction for SN 2011A is less than that of SN 1997bs. For SN 1997bs Van Dyk et al. (2000) derived a total extinction $A_V \sim 0.65$ mag. This value is close to that found for SN 2011A in Section 3.1.3 but not significantly lower.

Thanks to these comparisons and the fact that our spectrum taken 2.0 days after discovery has a good match with the SN 1994W spectrum taken 57 days past explosion, it is possible that SN 2011A exploded ∼50 days before discovery. Indeed, in both spectra we can see the presence of the same elements with identical line profiles, such as the Fe II multiplet λλ4923, 5018, 5169. This implies that the physical conditions for both spectra were similar and assuming that the evolution is not so different, the epochs are likely similar. This explosion date would then make the color curve between SN 2009kn and SN 2011A consistent (see Section 4.1). While the light curves are very similar between SN 2011A and SN 1997bs these are most likely related to CSM shells, and therefore any explosion date estimation is less reliable; the explosion date estimation from spectral comparisons is likely to be more valid.

4.2.2. Na I D Evolution

Na I D absorption can have three origins. From the ISM in the line of sight, the CSM ejected by the progenitor ionized by the radiation from the SN and recombined over the following several days to weeks, or from the SN ejecta. The main distinguishing feature between these three components is the velocity. If the absorption is due to the ISM, the velocity will be very low, ∼2–15 km s^{-1} (Fassia et al. 2001). If the component comes from the CSM, the velocity will be higher (few hundred km s^{-1} as for SN 2011A) and depends on the progenitor. Finally, the component from an SN ejecta would have the highest values of a few thousand km s^{-1}. Though the majority of spectra have low resolution and prevent us from resolving the Na I D absorption line, we believe that the absorption close to the Na I D wavelength position is mostly due to Na I D. Even if some lines like Ba II λ5854 can be blended with Na I D, the absorption strength and velocity are very rare. Indeed, other SNe have shown a similar remarkable increase of Na I D absorption, such as SN 1998A and SN 2009E (Pastorello et al. 2005, 2012), but Pastorello et al. (2013) measured the Na I D velocity for SN 2009E and found a value of ∼3000–5000 km s^{-1}. This implies that the absorption line is due the SN ejecta, whereas the velocities measured for Na I D absorption in SN 2011A never get higher than 1100 km s^{-1}, inconsistent with an ejecta origin, but consistent with a CSM origin interpretation.

In the literature we found a small number of cases of CSM Na I D in SNe IIn. Indeed for SN 2009kn (Kankare et al. 2012), SN 1994W (Chugai et al. 2004), SN 1997bs (Van Dyk et al. 2000), and SN 2005kj (Taddia et al. 2013), the velocity is low as for SN 2011A, less than 1100 km s^{-1}. The increase of Na I D absorption, according to Chugai & Danziger (1994), is a result of the increasing Na I ionization fraction.

4.2.3. Dust Formation

Most SN impostor candidates in the literature have no surviving star at the location of the transient, which could contradict the nature of the transient, i.e., non-terminal eruptions of massive stars. However, a simple reason could explain this. The dust formed in a dense shell ejected by the star will obscure the SN impostor. The presence of dust can be deduced in different ways. First, by the presence of an infrared excess due to the thermal emission from dust condensed in the ejecta or from heated pre-existing dust. Unfortunately, we do not have useful infrared data for this transient. Second, by

looking at the emission lines. If the spectral feature profiles show a blueshift, this can be attributed to the fact that the red side of the ejecta is blocked by the new dust (Smith et al. 2012, but see Anderson et al. 2014a and Dessart et al. 2015 for an alternative explanation). This effect is possibly seen in our transient. Indeed, in Figure 5 where the Hα emission line evolution is shown, we can see for the spectrum at +111.8 days that the red side is weaker compared to the blue part. This characteristic is not clearly observed after and before this epoch, especially because of the appearance of a P Cygni profile.

The estimated blackbody temperature at late times (3300 K) is also possibly indicative of dust formation. This is because this temperature appears to be too low for the spectra to be dominated by strong Balmer emission lines. This low temperature could be due to dust formation that reddens the object. Multi-band photometry fitting seems to favor an extincted blackbody, but it is difficult to put strong constraints on the blackbody temperature and extinction due to the small wavelength baseline and because our transient is mainly powered by interaction, which implies that using a blackbody fitting could be unrealistic. Any increase in reddening could also be related to the observed increase in Na I D. However, we note that the increase in the latter is more likely due to CSM effects.

4.2.4. CSM Properties

Analyzing the Hα emission line evolution with time together with the light curve allows us to constrain CSM properties. The SN 2011A light curve shows a double plateau. The presence of this rare double plateau leads us to speculate that the CSM is composed of two shells ejected by the pre-SN wind. Over ∼15 days there is an initial plateau that corresponds to the interaction between the SN blast wave and the first shell. When the ejecta reaches the edge of the first shell the light curve drops. If we assume that the blast wave speed is constant, and taking the value found in Section 3.2.3, ∼2000 km s^{-1}, we find a lower limit width of the first shell of ⩾2.6 × 10^{14} cm. It is a lower limit due to the fact that the beginning of this shell is not well constrained (because of the uncertainty in the explosion date). Then, there is another weaker plateau that lasts ∼15 days in the V band. Again, assuming that the ejecta velocity is constant with time, we find the width for the second shell, ∼2.6 × 10^{14} cm. A cartoon showing the CSM and the velocities of the different components is presented in Figure 16. This scenario would be similar to that proposed by Dessart et al. (2009) for SN 1994W.

This photometric analysis seems be also consistent with the spectral evolution. In Figure 5 we see that the Hα profile changes with time, from the very broad component at early epochs during the first plateau phase (spectra +2.0, +2.4, and +14.9 days), to a narrower broad component, accompanied with low-velocity Hα absorption (+56.8, +64, +70, +80.9, +85.9 days) during and after the second plateau.

5. CONCLUSIONS

We have presented a detailed study of SN 2011A, initially classified as an SN IIn based on the presence of narrow Hα emission in the spectrum. While the exact nature of the transient remains unclear, SN 2011A shows a number of interesting and unusual properties.

Figure 16. Cartoon illustration of the CSM composition with the velocity of the different components. The black star represents the transient. Not to scale.

1. A double plateau in light curve likely due to CSM composed of two shells.
2. Low luminosity, $-15.10 \geqslant M_V \geqslant -15.72$ (depending on the assumed host-galaxy extinction, 0 or 0.62 mag in the V band).
3. Low P Cygni Hα velocity $\leqslant 1200$ km s^{-1}.
4. Low-velocity absorption close to Na I D $\leqslant 1100$ km s^{-1}.
5. Variable absorption close to Na I D increasing in strength, from 3 to 10 Å in EW.

Given the photometric and spectroscopic properties we have derived for SN 2011A, most importantly its low luminosity and low ejecta velocity together with their comparison to other interacting transients, we believe that SN 2011A is most likely an SN impostor event. However, we also note that our analysis has demonstrated the difficulty in determining whether interacting transients are true terminal events or indeed SN impostors. The reader also must keep in mind that the characteristics used to separate the two events are in general arbitrary and hence detailed studies of future events are needed to further elucidate this issue.

REFERENCES

Abbott, D. C., & Conti, P. S. 1987, ARA&A, 25, 113
Adams, S. M., & Kochanek, C. S. 2015, arXiv:1502.00001
Anderson, J. P., Habergham, S. M., James, P. A., & Hamuy, M. 2012, MNRAS, 424, 1372
Anderson, J. P., Dessart, L., Gutiérrez, C. P., et al. 2014a, MNRAS, 441, 671
Anderson, J. P., González-Gaitán, S., Hamuy, M., et al. 2014b, ApJ, 786, 67
Arcavi, I., Gal-Yam, A., Yaron, O., et al. 2011, ApJL, 742, L18
Bond, H. E., Bedin, L. R., Bonanos, A. Z., et al. 2009, ApJL, 695, L154
Botticella, M. T., Pastorello, A., Smartt, S. J., et al. 2009, MNRAS, 398, 1041
Buzzoni, B., Delabre, B., Dekker, H., et al. 1984, Msngr, 38, 9
Campana, S., Mangano, V., Blustin, A. J., et al. 2006, Natur, 442, 1008
Cardelli, J. A., Clayton, G. C., & Mathis, J. S. 1989, ApJ, 345, 245
Chevalier, R. A. 1981, ApJ, 251, 259
Chugai, N. N. 1990, SvAL, 16, 457
Chugai, N. N. 2001, MNRAS, 326, 1448
Chugai, N. N., Blinnikov, S. I., Cumming, R. J., et al. 2004, MNRAS, 352, 1213
Chugai, N. N., & Danziger, I. J. 1994, MNRAS, 268, 173
Cortini, G., Villi, M., Barbon, R., et al. 1994, IAUC, 6042, 1
Crowther, P. A. 2007, ARA&A, 45, 177
Dessart, L., Audit, E., & Hillier, D. J. 2015, arXiv:1503.05463
Dessart, L., Hillier, D. J., Gezari, S., Basa, S., & Matheson, T. 2009, MNRAS, 394, 21
Dilday, B., Howell, D. A., Cenko, S. B., et al. 2012, Sci, 337, 942
Dwarkadas, V. V., Dewey, D., & Bauer, F. 2010, MNRAS, 407, 812
Faran, T., Poznanski, D., Filippenko, A. V., et al. 2014, MNRAS, 442, 844
Fassia, A., Meikle, W. P. S., Chugai, N., et al. 2001, MNRAS, 325, 907
Fassia, A., Meikle, W. P. S., Vacca, W. D., et al. 2000, MNRAS, 318, 1093
Filippenko, A. V. 1997, ARA&A, 35, 309
Fransson, C. 1982, A&A, 111, 140
Fraser, M., Inserra, C., Jerkstrand, A., et al. 2013, MNRAS, 433, 1312
Gal-Yam, A., & Leonard, D. C. 2009, Natur, 458, 865
Gräfener, G., & Hamann, W.-R. 2008, A&A, 482, 945
Groh, J. H., Meynet, G., & Ekström, S. 2013, A&A, 550, L7
Habergham, S. M., Anderson, J. P., James, P. A., & Lyman, J. D. 2014, MNRAS, 441, 2230
Hamuy, M. 2003, ApJ, 582, 905
Hamuy, M., Folatelli, G., Morrell, N. I., et al. 2006, PASP, 118, 2
Hamuy, M., Phillips, M. M., Suntzeff, N. B., et al. 2003, Natur, 424, 651

Hamuy, M., Suntzeff, N. B., Heathcote, S. R., et al. 1994, PASP, 106, 566
Hamuy, M., Walker, A. R., Suntzeff, N. B., et al. 1992, PASP, 104, 533
Humphreys, R. M., & Davidson, K. 1994, PASP, 106, 1025
Kankare, E., Ergon, M., Bufano, F., et al. 2012, MNRAS, 424, 855
Kiewe, M., Gal-Yam, A., Arcavi, I., et al. 2012, ApJ, 744, 10
Kochanek, C. S. 2011, ApJ, 741, 37
Landolt, A. U. 1992, AJ, 104, 340
Landolt, A. U. 2007, AJ, 133, 2502
Langer, N. 1993, SSRv, 66, 365
Li, W., Filippenko, A. V., van Dyk, S. D., et al. 2002, PASP, 114, 403
Maeder, A., & Meynet, G. 2008, in ASP Conf. Ser. 388, Mass Loss from Stars
    and the Evolution of Stellar Clusters, ed. A. de Koter, L. J. Smith &
    L. B. F. M. Waters (San Francisco, CA: ASP), 3
Maeder, A., Meynet, G., & Hirschi, R. 2005, in ASP Conf. Ser. 336, Cosmic
    Abundances as Records of Stellar Evolution and Nucleosynthesis, ed.
    T. G. Barnes, III & F. N. Bash (San Francisco, CA: ASP), 79
Margutti, R., Milisavljevic, D., Soderberg, A. M., et al. 2014, ApJ, 780, 21
Mauerhan, J. C., Smith, N., Filippenko, A. V., et al. 2013, MNRAS, 430, 1801
Maund, J. R., Smartt, S. J., Kudritzki, R.-P., et al. 2006, MNRAS, 369, 390
Mazzali, P. A., Deng, J., Hamuy, M., & Nomoto, K. 2009, ApJ, 703, 1624
Moriya, T. J., Maeda, K., Taddia, F., et al. 2014, MNRAS, 439, 2917
Nakar, E., & Piro, A. L. 2014, ApJ, 788, 193
Pastorello, A., Baron, E., Branch, D., et al. 2005, MNRAS, 360, 950
Pastorello, A., Botticella, M. T., Trundle, C., et al. 2010, MNRAS, 408, 181
Pastorello, A., Cappellaro, E., Inserra, C., et al. 2013, ApJ, 767, 1
Pastorello, A., Pumo, M. L., Navasardyan, H., et al. 2012, A&A, 537, A141
Pastorello, A., Zampieri, L., Turatto, M., et al. 2004, MNRAS, 347, 74
Patat, F. 1996, PhD thesis, Univ. Padova
Phillips, M. M., Simon, J. D., Morrell, N., et al. 2013, ApJ, 779, 38
Pignata, G., Maza, J., & Antezana, R. 2009, in AIP Conf. Ser. 1111 Probing
    Stellar Populations out to the Distant Universe: CEFALU 2008, ed. G.
    Giobbi et al. (Melville, NY: AIP), 551
Pignata, G., Cifuentes, M., Maza, J., et al. 2011, CBET, 2623, 1
Prieto, J. L., Brimacombe, J., Drake, A. J., & Howerton, S. 2013, ApJL,
    763, L27
Prieto, J. L., Sellgren, K., Thompson, T. A., & Kochanek, C. S. 2009, ApJ,
    705, 1425

Reichart, D., Nysewander, M., Moran, J., et al. 2005, NCimC, 28, 767
Richardson, D., Branch, D., Casebeer, D., et al. 2002, AJ, 123, 745
Richmond, M. W., Treffers, R. R., Filippenko, A. V., et al. 1994, AJ, 107,
    1022
Salamanca, I., Cid-Fernandes, R., Tenorio-Tagle, G., et al. 1998, MNRAS,
    300, L17
Schaller, G., Schaerer, D., Meynet, G., & Maeder, A. 1992, A&AS, 96,
    269
Schlafly, E. F., & Finkbeiner, D. P. 2011, ApJ, 737, 103
Schlegel, E. M. 1990, MNRAS, 244, 269
Smartt, S. J. 2009, ARA&A, 47, 63
Smartt, S. J. 2015, PASA, 32, 16
Smith, J. A., Tucker, D. L., Kent, S., et al. 2002, AJ, 123, 2121
Smith, N. 2013, MNRAS, 434, 102
Smith, N., Ganeshalingam, M., Chornock, R., et al. 2009, ApJL, 697, L49
Smith, N., Li, W., Foley, R. J., et al. 2007, ApJ, 666, 1116
Smith, N., Li, W., Silverman, J. M., et al. 2011, MNRAS, 415, 773
Smith, N., Mauerhan, J. C., & Prieto, J. L. 2014, MNRAS, 438, 1191
Smith, N., Silverman, J. M., Filippenko, A. V., et al. 2012, AJ, 143, 17
Smith, N., & Tombleson, R. 2015, MNRAS, 447, 598
Smith, N., & Townsend, R. H. D. 2007, ApJ, 666, 967
Sollerman, J., Cumming, R. J., & Lundqvist, P. 1998, ApJ, 493, 933
Steele, I. A., Smith, R. J., Rees, P. C., et al. 2004, Proc. SPIE, 5489, 679
Stothers, R. B., & Chin, C.-W. 1996, ApJ, 468, 842
Stritzinger, M., Prieto, J. L., Morrell, N., & Pignata, G. 2011, CBET, 2623, 2
Taddia, F., Stritzinger, M. D., Sollerman, J., et al. 2013, A&A, 555, A10
Tartaglia, L., Pastorello, A., Taubenberger, S., et al. 2015, MNRAS, 447,
    117
Theureau, G., Hanski, M. O., Coudreau, N., Hallet, N., & Martin, J.-M. 2007,
    A&A, 465, 71
Umeda, H., & Nomoto, K. 2008, ApJ, 673, 1014
Van Dyk, S. D., Li, W., Filippenko, A. V., et al. 2006, arXiv:astro-ph/0603025
Van Dyk, S. D., Peng, C. Y., King, J. Y., et al. 2000, PASP, 112, 1532
Vink, J. S. 2011, Ap&SS, 336, 163
Wagner, R. M., Vrba, F. J., Henden, A. A., et al. 2004, PASP, 116, 326
Weis, K., & Bomans, D. J. 2005, A&A, 429, L13
Zhang, T., Wang, X., Wu, C., et al. 2012, AJ, 144, 131